



The Dixon technique for MRI of the bone marrow

Niels van Vucht¹ · Rodney Santiago¹ · Bianca Lottmann¹ · Ian Pressney¹ · Dorothee Harder² · Adnan Sheikh³ · Asif Saifuddin¹

Received: 7 May 2019 / Revised: 25 June 2019 / Accepted: 27 June 2019 / Published online: 15 July 2019
© ISS 2019

Abstract

Dixon sequences are established as a reliable MRI technique that can be used for problem-solving in the assessment of bone marrow lesions. Unlike other fat suppression methods, Dixon techniques rely on the difference in resonance frequency between fat and water and in a single acquisition, fat only, water only, in-phase and out-of-phase images are acquired. This gives Dixon techniques the unique ability to quantify the amount of fat within a bone lesion, allowing discrimination between marrow-infiltrating and non-marrow-infiltrating lesions such as focal nodular marrow hyperplasia. Dixon can be used with gradient echo and spin echo techniques, both two-dimensional and three-dimensional imaging. Another advantage is its rapid acquisition time, especially when using traditional two-point Dixon gradient echo sequences. Overall, Dixon is a robust fat suppression method that can also be used with intravenous contrast agents. After reviewing the available literature, we would like to advocate the implementation of additional Dixon sequences as a problem-solving tool during the assessment of bone marrow pathology.

Keywords MRI · Dixon · Chemical shift imaging · Musculoskeletal diseases · Bone marrow pathology · Bone marrow assessment · Characterizing bone lesions · Quantitative bone lesion analysis

Introduction

The Dixon technique, named after its inventor, was first developed in 1984 [1]. The technique is well-known in abdominal radiology for distinguishing benign adrenal adenomas from other adrenal masses [2], and for detecting liver steatosis. It was first introduced for the assessment of bone marrow in 1985 by Wismer et al. [3], but struggled to find its clinical use. Today, chemical shift imaging (CSI) algorithms and Dixon-type pulse sequences are widely accepted and commonly offered as a standard fat-suppression technique by nearly every manufacturer, all with their specific patented names. For example, General Electric (GE) has iterative decomposition of water and fat with echo

asymmetry and least squares estimation (IDEAL), Siemens uses the generic name DIXON and Philips offers multi-point or mDixon [4]. The Dixon technique can be used with gradient echo (GRE) and spin echo (SE) sequences [5], both two-dimensional (2D) single-slice or three-dimensional (3D) parallel imaging. There are differences between the GRE and SE MRI techniques, including an overall faster scanning time using GRE, but GRE imaging of musculoskeletal tissues displays image contrast characteristics different from those of fast spin echo (FSE) pulse sequences, which are commonly used in the assessment of joints. This difference may limit their adoption in clinical practice as a viable replacement for standard 2D FSE pulse sequences [6]. Compared with 2D techniques, 3D MRI allows higher signal-to-noise ratio (SNR) producing better quality images. The SNR is higher with 3D techniques because each view during the acquisition contributes signal to every image in the entire volume. In contrast, with 2D single-slice techniques, each view contributes signal only to a given slice.

✉ Niels van Vucht
niels.vanvucht@nhs.net

¹ Department of Medical Imaging, Royal National Orthopaedic Hospital, Brockley Hill, Stanmore HA7 4LP, UK

² Clinic of Radiology and Nuclear Medicine, University Hospital Basel, University of Basel, Petersgraben 4, 4031 Basel, Switzerland

³ Department of Medical Imaging, The Ottawa Hospital, Civic Campus, 1053 Carling Avenue, Ottawa, Ontario K1Y 4E9, Canada

Fat suppression methods

Fat suppression techniques can be divided into three major categories:

1. Chemical shift-based fat suppression (chemical shift selective [CHESS], water excitation and Dixon)
2. Inversion-based fat suppression (short tau inversion recovery [STIR])
3. Hybrid techniques (spectral attenuated inversion recovery [SPAIR] and spectral pre-saturation with inversion recovery)

Each of these techniques has its own specific qualities.

With Dixon techniques, one echo (single-point Dixon) [7], two echoes (two-point Dixon) or more echoes (multi-point Dixon) are collected at different echo times (TEs) with specific echo spacing time, so that fat- and water-specific signals can be measured when they are in-phase (IP) and out-of-phase (OP). This gives Dixon its unique ability to quantify the amount of fat within a region of interest. By post-processing the IP and OP data, “water only” (WO) and “fat only” (FO) images are reconstructed [8]. Another strength of the Dixon technique is its outstanding homogeneity of fat suppression, because it is less sensitive to both main magnetic field (B₀) and radiofrequency field (B₁) heterogeneity compared with CHESS/fat-saturated methods, which gives even better results on higher magnetic fields (3.0 Tesla [3 T]) versus lower magnetic fields [9]. This makes Dixon an excellent technique for achieving uniform fat suppression (Fig. 1) [10]. The WO mDixon sequence at 3 T also demonstrates a reduction of metallic artefact around the knee compared with T2W FSE sequences [11].

Lee et al. showed that the FSE T2 Dixon sequence is superior to SPAIR owing to the quality of fat suppression, and to the delineation of lumbar spine lesions [12]. Brandão et al. [13] demonstrated more uniform fat suppression in the lumbar spine using three-point T1-weighted (T1W) and T2-weighted (T2W) Dixon compared with T1W fat suppressed (FS) and STIR, although there was no difference in lesion conspicuity. T1W and T2W IDEAL Dixon sequences have shown superior fat suppression compared to fat suppressed T1W and T2W FSE sequences for imaging the cervical spine (Fig. 2) and brachial plexus [14]. Rybicki et al. [15] compared 3-point Dixon with CHESS in the paediatric population, showing

superior fat suppression and lesion conspicuity particularly in the hands and feet. Superior fat suppression and SNR has also been demonstrated in the hands when comparing 3D fast spoiled gradient echo (FSPGR) T1W Dixon compared to CHESS sequences [16].

The Dixon imaging technique

Four different imaging sets

Understanding the technical background of CSI is essential in the interpretation of the four different imaging sets collected using Dixon techniques. These sequences are: IP (Fig. 3a), OP (Fig. 3b), FO (Fig. 3c) and WO (Fig. 3d). OP imaging has a notable feature that the organs and muscle compartments appear to be outlined with a “black pen” (Fig. 3b) owing to chemical shift artefact at a fat–water interface. The OP cancellation effect between fat and water gives rise to a specific type of MRI artefact called the “India ink artefact,” “black line artefact,” or so-called “chemical shift artefact of the second kind” [17].

Phase shift explained

A basic principle of MRI is that protons in a molecule precess at a specific frequency when placed in a magnetic field. Precession frequency is dependent on the strength of the external magnetic field and differs between 1.5 T and 3 T MRI units. Fat precesses more slowly than water, and at body temperature the precession frequency differences between fat and water are typically 210 Hz at 1.5 T and 420 Hz at 3 T [18]. The difference in resonance frequency, or spin rates between protons associated with fat molecules compared with those associated with water or other non-lipid molecules is termed “chemical shift” [19]. CSI relies on the phase shifts created by the fat–water spin resonance frequency difference to separate water from fat. During scanning, two sets of images are acquired with slightly different TEs. The first acquisition is performed at a TE with fat and water signals OP (Fig. 4), and

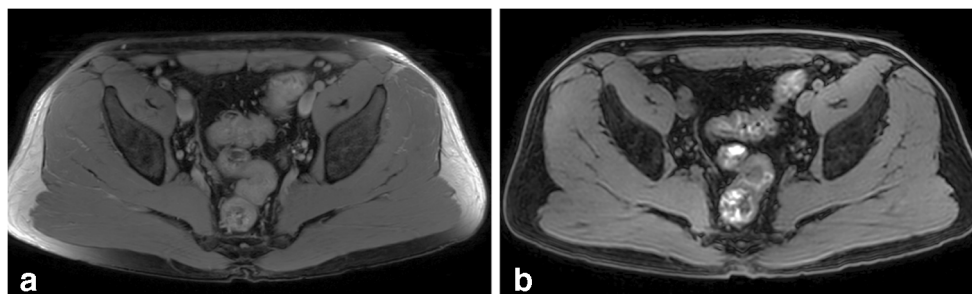


Fig. 1 Axial MRI through the pelvis in a 53-year-old man. **a** Spectral attenuated inversion recovery (SPAIR) image (recovery time [TR] = 3,000 ms; echo time [TE] = 30 ms) demonstrates poor suppression of

the subcutaneous fat on either side of the lower abdominal wall. **b** Water-only two-point gradient echo (GRE) T1-weighted (T1W) Dixon sequence demonstrates uniform suppression of the subcutaneous fat

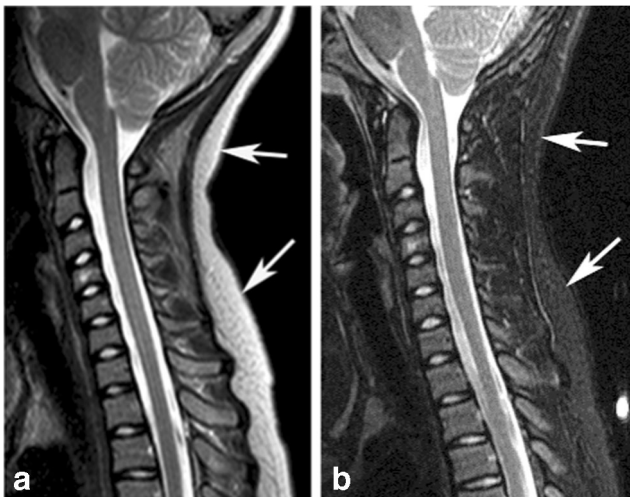


Fig. 2 Sagittal MRI of the cervical spine in an 11-year-old girl. **a** Short tau inversion recovery (STIR) image shows relatively poor suppression of the posterior subcutaneous fat (arrows). **b** Sagittal iterative decomposition of water and fat with echo asymmetry and least squares estimation (IDEAL) MR image (TR = 3,580 ms; TE = 114 ms) demonstrates excellent uniform suppression of the subcutaneous fat (arrows)

the second with the TE adjusted by a few milliseconds so that the fat and water signals are IP, corresponding to a TE difference of 2.2 ms at 1.5 T or 1.1 ms at 3 T [18].

The signal intensity (SI) is formed by the sum of signals from the fat and water spins. When the protons are in the same location (IP), the signals received from fat and water protons in the same voxel are additive (IP SI = water signal contribution + fat signal contribution). When they are in completely opposing phases (OP), the signals at least partially cancel each other out (Fig. 5; OP SI = water signal contribution – fat signal

contribution). This causes a decrease in SI on OP images in tissues that contain microscopic fat, which then appear darker than they do on their corresponding IP images (Fig. 6). Through post-processing, the WO and FO images can be reconstructed by adding and subtracting the signal IP (SIP) and signal OP (SOP) respectively [8, 18, 19]. By combining SIP and SOP, the WO images are obtained— $WO = (SIP+SOP)/2$. By subtracting SOP from SIP, the FO image is produced— $FO = (SIP-SOP)/2$. In this way, both fat-suppressed and non-fat-suppressed images are acquired simultaneously.

Two-point Dixon and multi-point Dixon

The original two-point technique described by Dixon [1] uses only two acquisitions with different TEs, producing IP and OP images. The use of three-point or six-point Dixon (multi-point Dixon), a third echo or more echoes are introduced. As a result, “purer” fat and water images are acquired independent of any field heterogeneity. Only when fat and water signals are accurately opposed, the IP and OP images do not suffer from unwanted signal contribution, leading to decreased reliability of calculations of SI decrease. Therefore, to achieve optimal signal difference, it is essential that exact IP and OP echo timing is acquired; otherwise, fat and water are only partially opposed [20], especially when using the two-point Dixon technique. However, some authors state that the TEs need not be limited to specific IP and OP conditions, and sequence timing can be more flexible as long as three or more echoes are acquired and proper fat dephasing coefficients are used [21]. When using three- or six-point Dixon, the total scan time will be at least tripled to that of a regular acquisition, which may be

Fig. 3 Coronal two-point GRE T1W Dixon MR images of the left femur of a 55-year-old man with myeloma. **a** In-phase (IP), **b** out-of-phase (OP), **c** fat-only and **d** water-only images showing a large lesion in the femoral diaphysis (arrows) and a small tumour nodule more distally. Note the “India ink artefact” on the OP image (**b**)

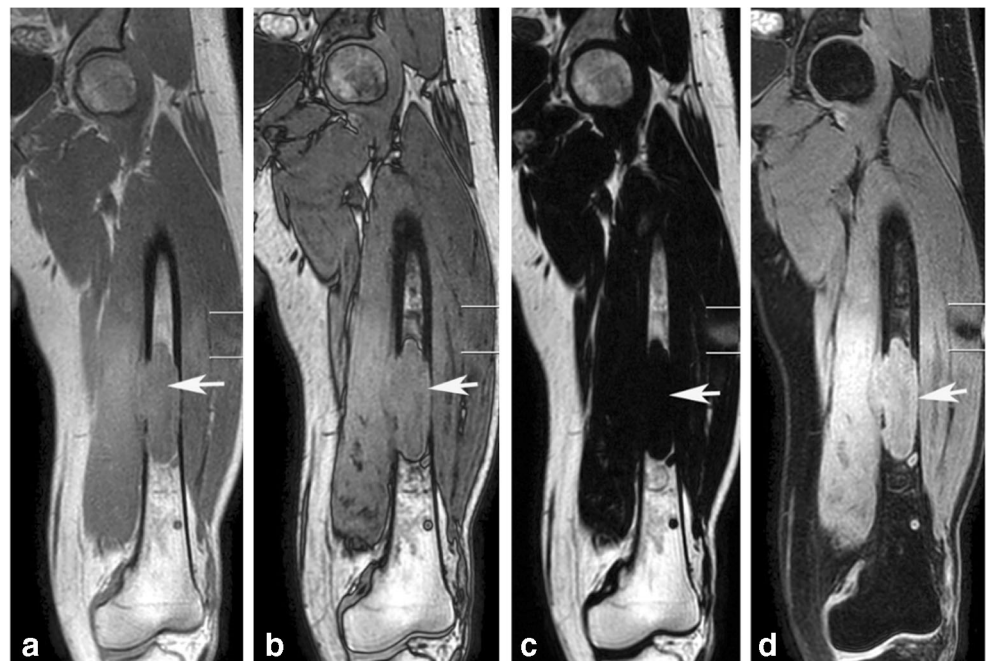
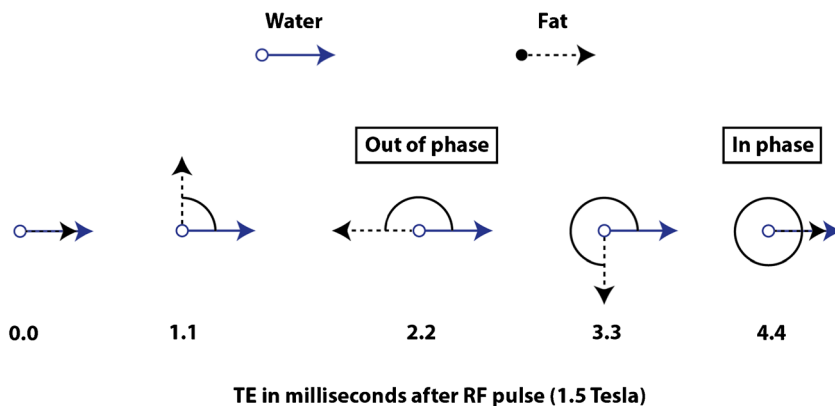


Fig. 4 Phase-cycling between fat and water protons. IP and OP conditions occur twice per cycle, approximately every 2.2 ms at 1.5 T



an undesirable consequence [22]. However, the lengthened scanning time results in increased SNR compared with a single acquisition, leading to better image quality [23].

Reduced scanning times

The original Dixon technique was a relatively long sequence as it acquired multiple images at fixed TEs, but when using GRE two-point Dixon, scanning times are generally very fast. Using T2W FSE Dixon can replace both T2W FSE and SPAIR or other fat suppression acquisitions [12], which can save further on total scan time. Maeder et al. [5] showed that the combination of T2W SE Dixon FO and WO could eliminate the need for a conventional T1W SE sequence reducing total scanning time. The FSE three-point Dixon technique has been compared with conventional FSE T2W sequences at 3 T for MRI of the knee, showing no significant difference in diagnostic performance and allowing a reduction in scan times [24].

Quantification techniques

A variety of methods have been used to quantify the degree of fat within a marrow lesion. One of the most frequently used is the measurement of SI decrease on OP images compared with IP images. Identical regions of interest (ROIs) are drawn in the bone on IP and OP images and the percentage decrease is measured as follows: $((SIP-SOP)/SIP) \times 100 = \text{SI drop } \%$. At 1.5 T, an SI decrease $>20\%$ is said to be consistent with a benign fat-containing marrow lesion, whereas a decrease $<20\%$ is consistent with replacement of marrow fat owing to a malignant process [25–28].

Zampa et al. [29] compared T1W SE and OP GRE images to calculate the SI ratio as follows: $\text{SI ratio} = \text{OP GRE SI}/\text{T1W SE SI}$. A SI ratio > 1 was considered consistent with malignancy, as it indicated little or no fat in the ROI. Also, Costa et al. [30] calculated relative SI ratios between OP and IP GRE images with a ratio of >1 indicative of a neoplastic process, whereas a ratio of <1 was indicative of fat within the lesion and therefore a non-neoplastic process.

Fig. 5 Signal vector diagram describing the observed signal in chemical shift imaging (CSI). For the IP and OP images, the signal of water and fat is added and the resultant signal is observed. Water and fat images can then be generated by adding and subtracting the IP and the OP images respectively

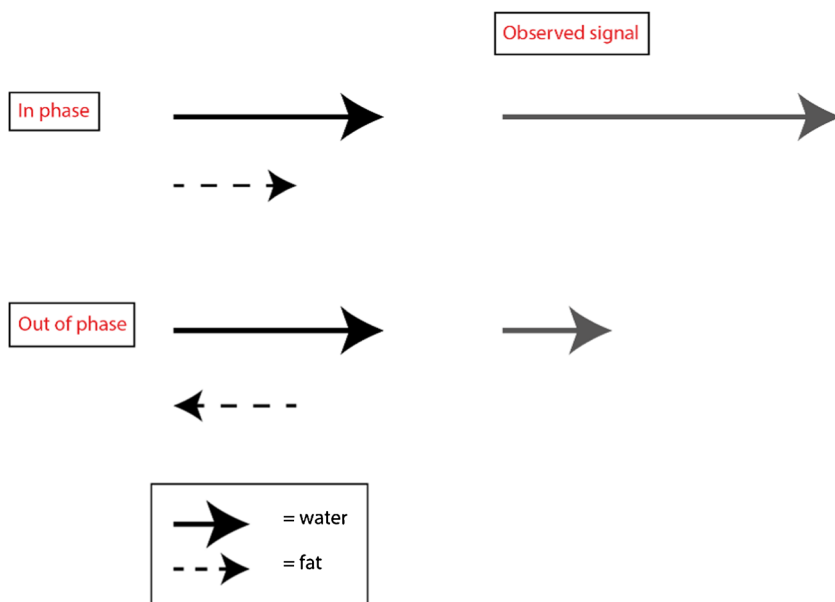
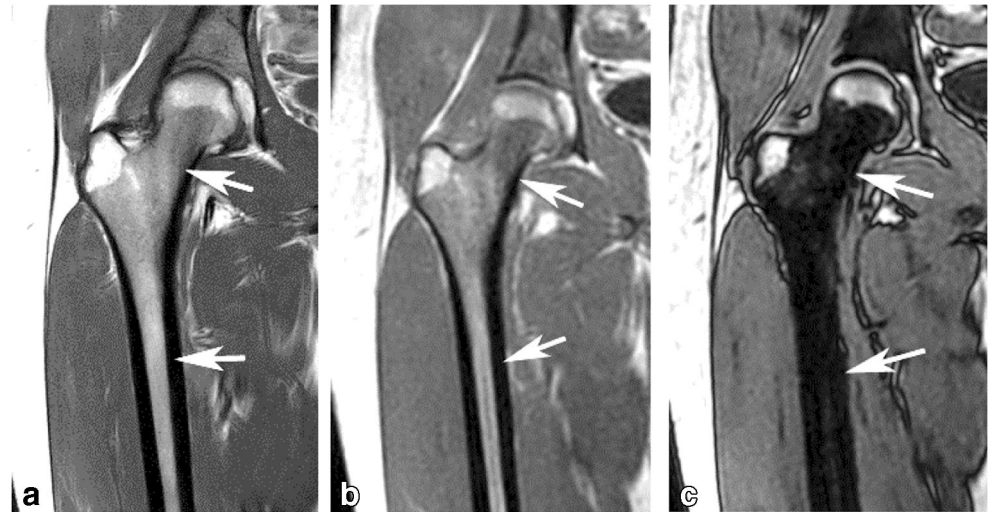


Fig. 6 Coronal MRI of the right proximal femur of a 23-year-old woman. **a** T1W TSE and **b** IP Dixon images show intermediate marrow SI due to hyperplastic red marrow (*arrows*). Note that it remains hyperintense compared with skeletal muscle on T1W TSE (**a**). **c** OP image shows a profound reduction of marrow SI owing to its high fat content (*arrows*)



Proton density fat fraction (PDFF), which equals fat/(water + fat) has been used with a six-echo GRE modified Dixon sequence at 3 T to differentiate benign from malignant vertebral lesions [31], and acute benign compression fractures from pathological vertebral fractures [32]. In both cases, the benign pathology had significantly higher PDFF than malignant lesions. Using the same MRI technique, T2* relaxation times and T2* ratio (fracture T2*/normal vertebrae T2*) have also been used to differentiate benign from malignant vertebral collapse, with both measurements being significantly higher for malignant lesions [33].

Clinical applications of the Dixon technique

The varied clinical applications of the Dixon technique have been recently reviewed by Pezeshk et al. [34]. Most studies have focused on its use in the differentiation between benign and malignant focal vertebral lesions. In a meta-analysis, Suh et al. [35] showed that CSI had pooled sensitivity and specificity of 92% and 87% in this clinical setting. Diagnostic accuracy increased by the use of CSI with short TE and low flip angle, and the Dixon method.

Bone marrow assessment and quantitative bone lesion analysis

In 1997, Carroll et al. showed with high sensitivity and specificity that on T1W SE MRI, skeletal muscle and intervertebral disk serve as internal standards for differentiating infiltrative marrow pathology, which would be isointense, from normal hematopoietic marrow, which would be slightly hyperintense (Fig. 6) [36]. With Dixon, it is now possible to use quantification to help predict the nature of a bone marrow lesion [29, 37], potentially eliminating the requirement for

biopsy in more than 60% of patients with non-neoplastic disease (Fig. 7) [25].

Hematopoietic red marrow

At birth, the whole skeleton is composed of hematopoietic red marrow that gradually matures to yellow fatty marrow. Red and yellow bone marrow have different cellular and chemical composition [38, 39], which form the basis of CSI and differentiating between bone marrow abnormalities. Red bone marrow reconversion refers to the process of fatty marrow being replaced by red marrow owing to a variety of causes including obesity, diabetes and anaemia, and non-medical conditions such as smoking and sports that require a large oxygen debt (long-distance running, free diving). When red marrow is abundant, T1W marrow signal is reduced, making it potentially difficult to differentiate from areas of neoplastic infiltration [40].

In normal bone marrow, which contains both fat and water protons in a single voxel, a significant signal loss occurs on the OP images relative to the IP images (Fig. 6) [25, 26, 34, 41–43]. At 1.5 T, a signal drop of approximately 20% on the OP imaging is generally accepted as the cut-off level to distinguish normal marrow from marrow infiltration. Disler et al. [44] reported that less than 19% SI drop on 1.5 T OP imaging has a sensitivity and specificity of 95% for the detection of neoplasm. The optimal threshold has also been studied at 3 T, Kumar et al. showing that a threshold SI decrease of 25% produced at least 100% sensitivity and 86% specificity for identifying marrow replacement [45]. They state that differences in the impact of T2* effects and the increased SNR at 3 T relative to 1.5 T may account for the differences in CSI measurements at different field strengths.

Primary or metastatic bone lesions replace normal bone marrow, leading to the replacement of normal fatty marrow signal [44, 46, 47]. When a voxel contains tumour replacing

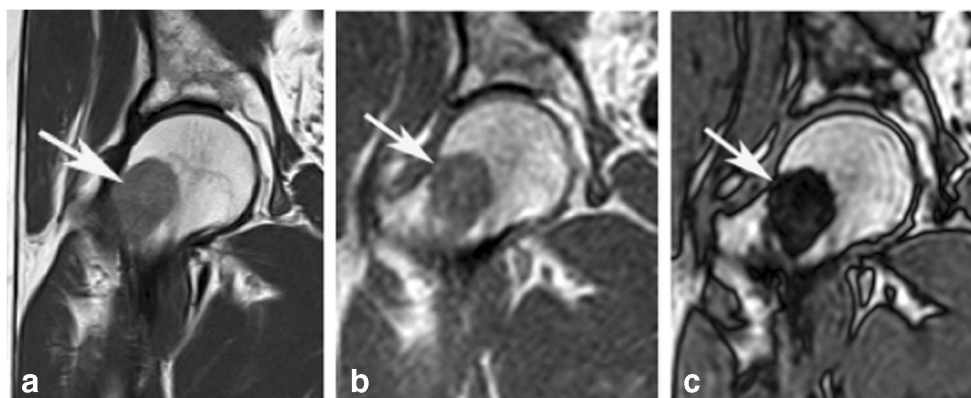


Fig. 7 Coronal MRI of the right proximal femur of a 72-year-old male with prostate cancer. **a** T1W TSE MRI shows a well-defined hypointense lesion in the femoral neck (*arrow*) referred for biopsy to investigate the possibility of metastasis. **b** IP Dixon image shows an intermediate

marrow SI lesion (*arrow*). **c** OP image shows profound reduction of marrow SI owing to its high fat content (*arrow*). The SI drop was calculated at 73%. A diagnosis of focal nodular marrow hyperplasia was made, and biopsy was not performed

normal fat containing marrow, water signal remains and there will be no significant signal decrease on the OP imaging. The common non-malignant conditions that alter normal fatty marrow MR signal include: red marrow reversion, focal nodular marrow hyperplasia (FNMH), intra-osseous haemangioma and marrow oedema of any cause (i.e. trauma, inflammation). In these situations, there is typically enough preservation of fat to allow a >20% (1.5 T) or >25% (3.0 T) signal loss on OP imaging [44].

Focal nodular marrow hyperplasia

Focal nodular marrow hyperplasia (FNMH) is a not uncommon, incidentally observed marrow lesion that can mimic metastasis [48, 49]. It is usually seen in middle-aged or elderly patients and typically in the spine [48], although the pelvis and proximal femur are also relatively common locations. FNMH classically demonstrates reduced SI on both T1W and T2W FSE sequences and may be mildly hyperdense on CT, but typically shows no increased activity on bone scintigraphy. However, it may be active on FDG-PET [48]. Although T1W SE SI being slightly higher than that of skeletal muscle is suggestive of the diagnosis, CSI is ideally suited to clarifying the nature of these lesions [43, 50] owing to their relatively high fat content, as illustrated by Douis et al. (Figs. 7, 8) [27]. However, we are unaware of any study that has determined the diagnostic accuracy of CSI for the diagnosis of FNMH.

Intra-osseous haemangioma

Intra-osseous haemangiomas are slow-growing and generally asymptomatic benign neoplasms that are commonly found in the vertebral bodies [51]. They consist of thin-walled sinusoidal channels lined by vascular endothelium with interspersed bony trabeculae, containing a variable amount of fat. Typical haemangiomas show T1W hyperintensity due to fatty stroma

with T2W hyperintensity due to vascularity, and are easily recognised. However, atypical or lipid-poor haemangiomas comprise mostly vascular soft tissue and contain only small or microscopic amounts of fat, thus demonstrating intermediate-to-low T1W SI compared with skeletal muscle and therefore potentially posing a diagnostic dilemma [52]. Dynamic contrast-enhanced MRI (DCE-MRI) has been used successfully to differentiate atypical haemangiomas from metastases based on difference in SI and time–intensity curves [53]. CSI is also helpful, since atypical haemangiomas usually show >20% signal drop on (1.5 T) OP imaging owing to their microscopic fat content (Fig. 9) [26]. Shi et al. compared T1W SE, CSI, diffusion-weighted imaging (DWI) and contrast-enhanced MRI in the differentiation of atypical haemangiomas from metastases, CSI demonstrating a diagnostic accuracy of ~85% [54]. However, difficulty can arise in atypical haemangiomas that are relatively sclerotic, in which case the SI drop on (1.5 T) OP images may be <20%, resulting in a false-positive diagnosis of malignancy. Other benign lesions associated with marrow sclerosis, such as fracture callus (Fig. 10) and Paget’s disease may produce similar findings (Fig. 11). Therefore, if a lesion that has features that are not particularly concerning with regard to malignancy on routine MRI, but shows <20% SI decrease or increase on (1.5 T) OP imaging, we routinely perform CT to identify whether or not the lesion is sclerotic.

Differentiation of non-pathological from pathological vertebral fractures

Abnormal SI in acute benign vertebral compression fractures (BVCFs) on conventional MRI can be like that seen in vertebrae with pathological fracture due to underlying malignancy [55]. A variety of MRI findings have been described to distinguish between the two entities [56, 57]. SI differences between IP and OP images can guide in the differentiation

Fig. 8 A 51-year-old man with low back pain. **a** Sagittal T1W TSE and **b** coronal T2W FSE MRI show an oval hypointense lesion in the superior aspect of the L4 vertebral body (*arrows*). **c** Axial IP and **d** OP two-point Dixon GRE MRI demonstrate a 28.4% SI decrease on the OP images indicative of a fat-containing lesion. The combined imaging features would be consistent with focal nodular marrow hyperplasia. The numbers (648 and 464) stand for measured SI (Signal Intensity)

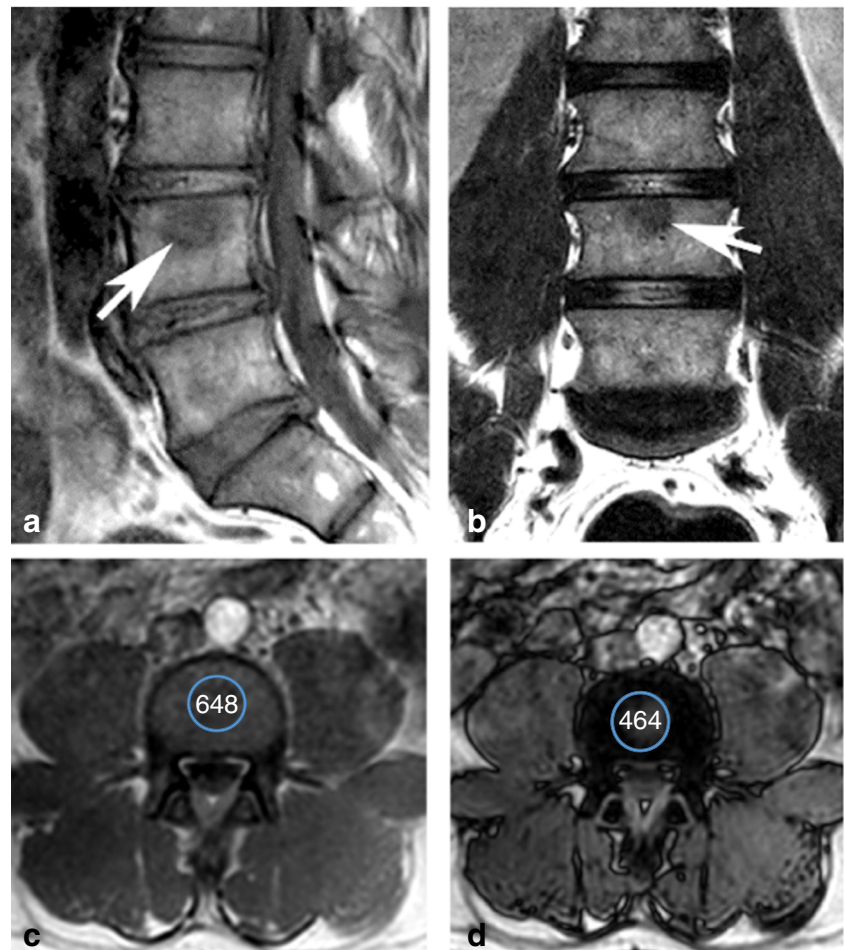
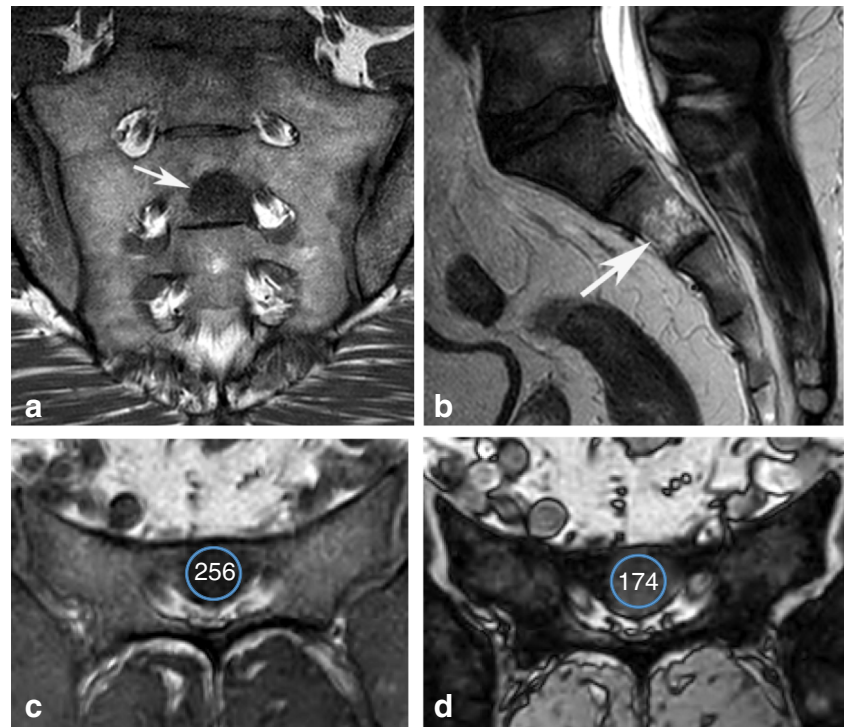


Fig. 9 A 44-year-old man with an incidental lesion noted in the S2 sacral segment. **a** Coronal T1W TSE and **b** sagittal T2W FSE MR images showing a lobular lesion in the upper sacrum, which is hypointense on T1W (*arrow* in **a**) and hyperintense on T2W (*arrow* in **b**). **c** Axial IP and **d** OP two-point Dixon GRE MRI demonstrate an SI decrease of 32% on the OP images, indicative of a fat-containing lesion. The combined imaging features would be consistent with an atypical haemangioma. The numbers (256 and 174) stand for measured SI (Signal Intensity)



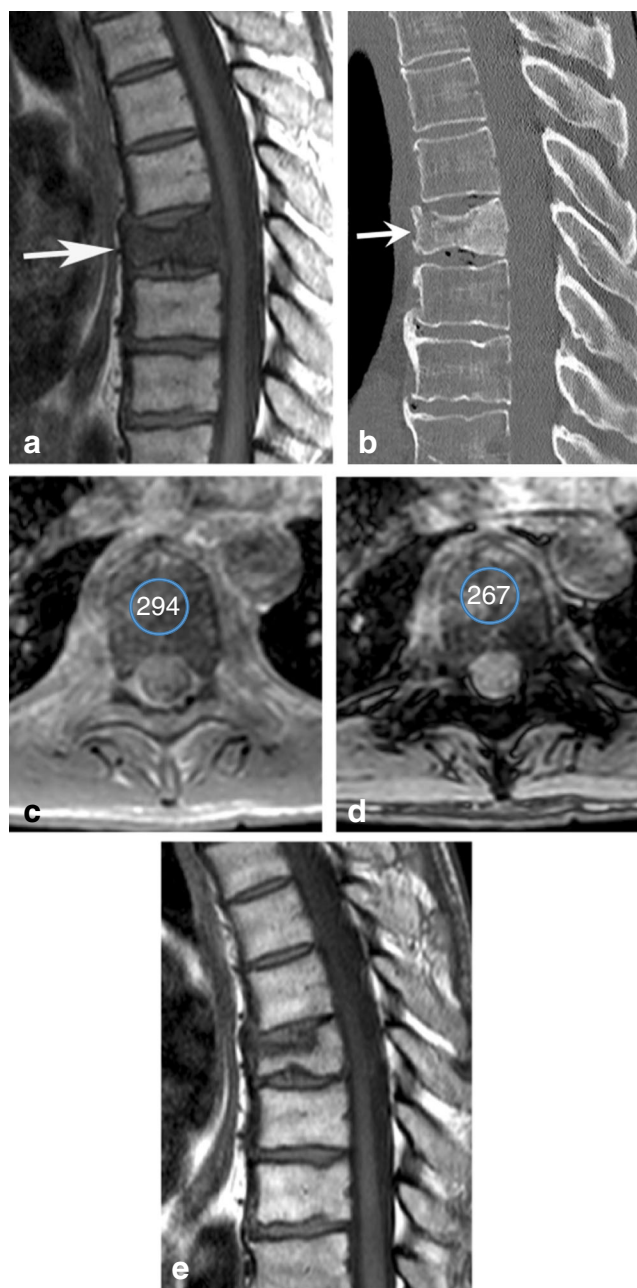


Fig. 10 A 64-year-old man with acute onset mid-thoracic back pain. **a** Sagittal T1W TSE MRI shows diffuse reduction of marrow SI and collapse of the vertebral body, raising the possibility of pathological collapse (*arrow*). **b** Sagittal CT MPR demonstrates vertebral collapse and associated marrow sclerosis (*arrow*). **c** IP and **d** OP axial two-point GRE Dixon MRI through the vertebra show an SI decrease of only 9.2%, consistent with malignant marrow infiltration. **e** Sagittal T1W TSE MRI obtained 3 months later shows almost complete healing of the vertebra, consistent with a benign vertebral compression fracture. The numbers (294 and 267) stand for measured SI (Signal Intensity)

between BVCFs and neoplastic vertebral compression fractures [58]. Erly et al. [59] and Geith et al. [28] demonstrated statistically significant differences in SI between quantitative IP and OP CSI for BVCFs and malignant compression fractures. Additionally, it has been shown that PDFF and PDFF

ratios of malignant compression fractures derived using the multipoint Dixon method are significantly lower than those of acute BVCFs, further allowing differentiation of the two fracture types [32, 43, 50, 55]. Ragab et al. [60] suggested that a decrease in SI >35% on (1.0 T–1.5 T) OP images compared with IP images might be used as a cut-off value to differentiate osteoporotic from pathological vertebral compression. This differentiation can also be achieved by calculating T2* relaxation times and T2* ratios, which are significantly higher for pathological fractures, with a reported accuracy of 73% and 89% respectively [33].

Defining the intra-osseous extent of a bone tumour

The evaluation of the extent of a bone lesion can be complicated by the presence of associated oedema-like marrow SI or abundant red marrow adjacent to the lesion, which is particularly problematic in the paediatric population. In general, fluid-sensitive sequences tend to overestimate tumour extent owing to the presence of perilesional oedema, which may have similar SI [40, 61]. Non-contrast T1W SE sequences are often used to identify the intra-medullary extent of a bone tumour, as this gives the best contrast between normal hyperintense fatty marrow and tumour tissue with intermediate SI [62]. If there is still ambiguity, contrast-enhanced fat-suppressed imaging can be performed, although areas of perilesional oedema may also enhance, which would again potentially overestimate tumour margins. Dixon imaging, and in particular the OP sequence, can show the extent of an intramedullary tumour with a high level of confidence and has been considered an alternative technique to T1W SE sequences [40, 61]. The exact determination of tumour margins is important to aid planning of resection level, particularly in the paediatric population, where sparing of the growth plate may allow the joint to be salvaged (Fig. 12).

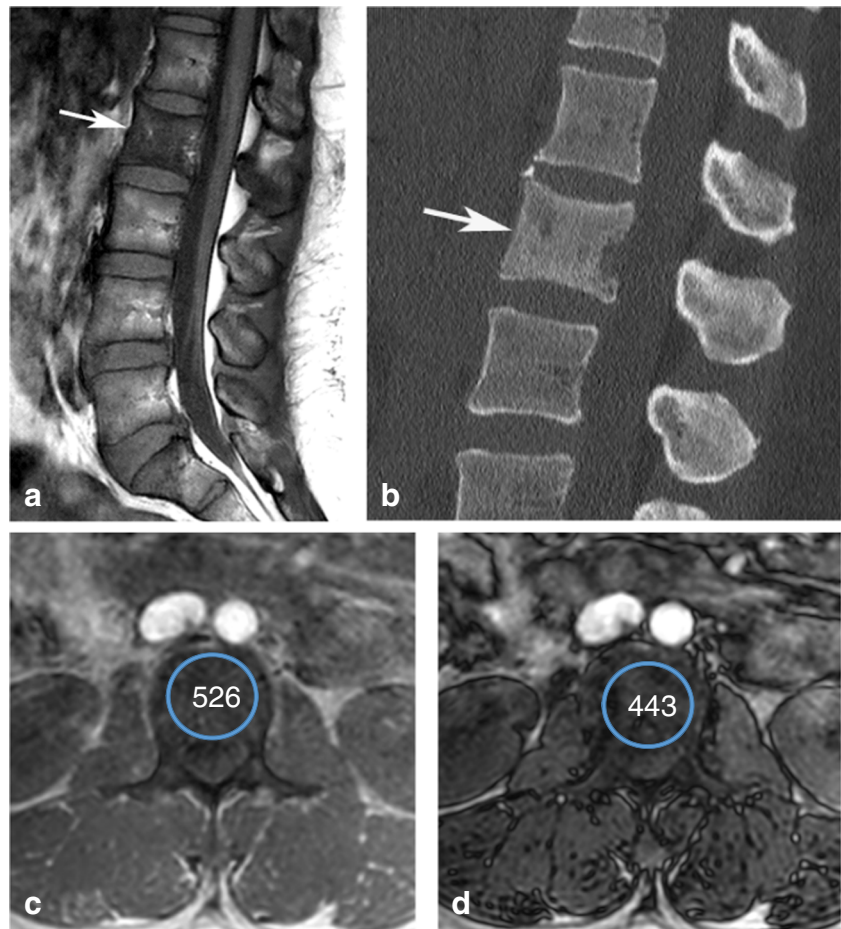
Haematological disorders

The Dixon technique has been used for imaging of haematological disorders, such as screening for multiple myeloma (MM), where FO images offer a higher lesion detection rate compared with IP images alone [63]. Signal drop on the OP imaging can be seen, consistent with fatty metamorphosis of healed MM lesions [34], which can be helpful if the typical findings of a healing lesion, such as a T1 peripheral fatty halo, are absent [64]. The combination of high accuracy for the detection of marrow-replacing lesions and fast acquisition times makes this a competitor to the conventional scanning methods.

Assessment of skeletal metastases

Magnetic resonance imaging has long been established as a highly sensitive and specific technique for the detection of

Fig. 11 Paget's disease involving the L2 vertebra in a 46-year-old woman. **a** Sagittal T1W TSE MRI shows heterogeneous reduction of marrow SI (*arrow*). **b** Sagittal CT MPR demonstrates marrow sclerosis and vertebral body enlargement (*arrow*). **c** Axial IP and **d** OP images show an SI decrease of 15.8% on OP, consistent with marrow infiltration. The numbers (526 and 443) stand for measured SI (Signal Intensity)



skeletal metastases from a wide variety of primary sites using a combination of T1W/T2W SE, STIR, GRE, DWI and contrast-enhanced imaging [65, 66]. More recently, the potential of Dixon sequences for the detection of skeletal metastases has been assessed. Maeder et al. [5] showed that the combination of T2W SE Dixon FO and WO was comparable with their standard protocol of T1W SE and T2W SE Dixon sequences in the assessment of potential vertebral metastases. The FO sequence was also found to significantly increase lesion conspicuity compared with T1W SE images. Similar findings were reported by Hahn et al. [67]. T1W OP GRE imaging has also been used to assess potential vertebral metastases at 0.2 T [68]. As with myeloma, changes in bone marrow fat–water ratio within healing skeletal metastases can be detected [69].

The detection of melanoma metastases is also more reliable on T2W SE Dixon FO images [5], which show a consistent loss of SI compared with the classical hyperintensity on T1W SE sequences, as melanin shortens T1, resulting in hyperintensity potentially obscuring melanoma metastases within the underlying hyperintense fatty marrow. Conversely, the differentiation

between a relatively hyperintense T1W melanoma metastasis and FNMH can also be made by the SI decrease seen in the latter on OP CSI (Fig. 13).

Over the last decade, whole-body MRI (WB-MRI) has become a well-established technique in the assessment of skeletal metastatic disease, comparing very favourably with skeletal scintigraphy in both the adult and paediatric populations [70–74]. More recently, the value of whole-body Dixon techniques has been reported [75]. Costelloe et al. [76] showed that the Dixon technique is suitable for whole-body bone metastasis screening as an alternative to skeletal scintigraphy, being highly specific (98.7% vs 89.1%) and more sensitive. Additionally, liver metastases were detected. The same authors evaluated a series of Dixon sequences for conspicuity of metastases, showing a significant improvement in conspicuity on fat-suppressed and FO T1W sequences with contrast enhancement [77].

Assessment of primary bone tumours

Characterisation of primary bone tumours remains initially within the realms of radiography [78, 79], the major use of



Fig. 12 A 12-year-old boy with a left femoral diaphyseal Ewing sarcoma. **a** Coronal T1W TSE MRI shows indistinct tumour margins (arrows) due to adjacent mild marrow hypointensity from a combination of reactive oedema and residual red marrow. **b** Coronal OP two-point GRE Dixon MRI shows a much clearer demarcation of the tumour (arrow) from the adjacent reactive marrow (thin arrows) owing to the high fat content of the latter causing a marked decrease in marrow SI

MRI being in local staging [62, 80, 81]. However, MRI also plays a role in the further characterisation of bone lesions [82], and in planning image-guided needle biopsy [83]. Currently, the use of the Dixon sequence in assessing primary bone

tumours is limited, although its potential for determining intra-osseous extent has already been mentioned.

Costa et al. [30] described the use of CSI in the assessment of osteoid osteoma (OO) in 17 patients with a proven histological diagnosis. They measured SI ratios on IP and OP images in three regions of interest, the nidus, the surrounding abnormal marrow and normal marrow. As expected, the mean SI ratio for the nidus was 1.2, consistent with a solid, possibly calcified lesion, and 0.35 for the surrounding marrow, consistent with marrow oedema. It is unclear how this aided the diagnosis, considering that CT had demonstrated the nidus in all cases.

Kenneally et al. [41] evaluated the addition of IP and OP CSI to standard MRI sequences in 27 bone lesions, 10 malignant and 17 non-malignant. Malignant lesions showed an overall mean SI drop of 0.69%, whereas benign lesions showed an overall mean SI decrease of 37.1%. The confidence for differentiating benign from malignant lesions increased with the addition of CSI. The authors concluded that CSI was of value in differentiating benign from malignant bone lesions. However, the group of benign lesions included only 8 benign tumours, 2 OOs and 6 presumed haemangiomas where the value of CSI is already established, and the SI decrease is due to either microscopic intra-lesional fat (haemangioma) or marrow oedema (OO) [41]. It is expected that benign tumours that replace the marrow would also show an SI drop <20% (on 1.5 T) and would therefore be indistinguishable from malignant lesions by CSI (Fig. 14). Further studies will be required with larger numbers and a greater variety of benign tumours to determine the role of CSI in distinguishing between benign and malignant primary bone tumours.

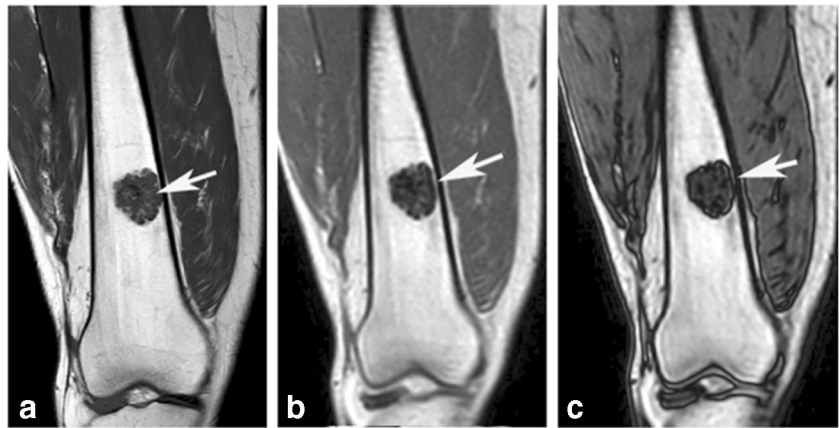
Assessment of osteoporosis

Osteoporosis results from decreased bone mass and quality and results in increased fracture risk. Quantification of bone mineral density (BMD) with techniques such as dual-energy

Fig. 13 A 61-year-old man with known malignant melanoma. **a** Coronal T1W TSE, **b** IP and **c** OP two-point GRE Dixon MRI showing a lesion in the proximal femur, suggestive of T1W hyperintense metastasis (arrow in **a**). The lesion shows similar SI on the IP sequence (arrow in **b**), but a profound decrease in SI on the OP sequence (arrow in **c**), indicative of high fat content due to FNMH rather than marrow-replacing metastasis



Fig. 14 A 36-year-old woman with a distal femoral enchondroma. **a** Coronal T1W TSE, **b** IP and **c** OP two-point GRE Dixon MRI showing a lobular intermediate SI lesion with similar morphology on all three sequences (*arrows*). The SI decrease on OP images was only 15%



X-ray absorptiometry (DEXA) and quantitative computed tomography (QCT) are well-established in the assessment of osteoporosis [84]. MRI techniques utilised for the assessment of osteoporosis include MR spectroscopy, DWI, DCE-MRI and CSI [84]. Osteoporosis is associated with an increase in bone marrow fat, and the inverse relationship between marrow fat and BMD has been demonstrated with hydrogen proton magnetic resonance ($^1\text{H-MR}$) spectroscopy [85]. Similarly, the bone marrow fat fraction (BMFF) obtained from modified Dixon techniques at 3 T may be used to predict abnormal BMD. Zhao et al. [86] found a significant difference in the BMFF in the lumbar spine among patients with normal BMD, with osteopenia and with osteoporosis using QCT as the reference standard.

Limitations and pitfalls of the Dixon technique

Modern Dixon techniques also have limitations. They do not completely solve the issues related to artefact in highly heterogeneous areas, such as around metallic hardware that are still present and can impede proper assessment. STIR sequences in some cases are still more reliable when it comes to fat suppression around large metallic prostheses [8].

Another interesting phenomenon is the so-called “fat–water swapping artefact”. This artefact occurs when a computational error in areas of field heterogeneity result in incorrect determination of whether a voxel contains water or fat. In this way, it converges to the wrong substance producing a water-only image when a fat-only image is desired. The images have geographic regions of inappropriate suppression with sharp margins. To overcome this problem, a third echo could be added to compensate for field heterogeneity, which makes this technique more robust at the expense of scan time [87].

When it comes to measuring the fat fraction and characterising bone lesions, it becomes apparent that this technique is very susceptible to subtle changes in scanning

parameters and that there are many variables that can influence the measurements on IP and OP imaging. For example, field strength, TE and flip angle all influence the final signal acquired [88]. A thorough understanding of the MRI technique is mandatory for producing reliable and accurate measurements.

During the implementation of the Dixon protocol in our institution, we have encountered lesions demonstrating an SI increase on OP imaging. This is typically found with sclerotic bone lesions such as myelofibrosis and from compacted bone in healing fractures. This phenomenon has also been described by Swartz and Roberts [89], who presented a case of a false-positive pelvic lesion with imaging features consistent with marrow fibrosis. For this reason, some sclerotic fat-containing marrow lesions, such as atypical haemangiomas and Paget’s disease, may also produce insufficient SI decrease on the OP images to allow differentiation from marrow infiltrative lesions (Figs. 10, 11).

Other potential false-positive and false-negative pitfalls include infiltrative multiple myeloma, haematoma in fracture sites, marrow-replacing benign cysts or geodes, magnetic susceptibility artefact of densely sclerotic metastases and renal cell carcinoma metastases containing fat [89]. Kenneally et al. [41] also reported that 6 out of 10 malignant lesions demonstrated an increase in SI, but did not go into detail as to why this phenomenon occurred. According to Maeder et al. [5], most false-negative and false-positive findings were due to previously treated metastases. Indeed, previous chemotherapy or radiotherapy may induce the appearance of intralesional fat, which could lead to false-negative results. This pitfall must be kept in mind when bone marrow imaging results are being reported.

Conclusions

Dixon imaging is a useful technique for characterising bone lesions by quantifying the amount of microscopic intracellular

fat. Its utility in marrow evaluation is well-recognised, with a reported sensitivity and specificity of up to 95% in predicting the likelihood of lesions being either neoplastic or non-neoplastic.

References

- Dixon WT. Simple proton spectroscopic imaging. *Radiology*. 1984;153(1):189–94.
- Adam SZ, Nikolaidis P, Horowitz JM, Gabriel H, Hammond NA, Patel T, et al. Chemical shift MR imaging of the adrenal gland: principles, pitfalls, and applications. *RadioGraphics*. 2016;36(2):414–32.
- Wisner GL, Rosen BR, Buxton R, Stark DD, Brady TJ. Chemical shift imaging of bone marrow: preliminary experience. *Am J Roentgenol*. 1985;145:1031–7.
- Lefebvre G. One sequence, many benefits in musculoskeletal MRI. *Fieldstrength*. 2015:18–21.
- Maeder Y, Dunet V, Richard R, Becce F, Omoumi P. Bone marrow metastases: T2-weighted Dixon spin-echo fat images can replace T1-weighted spin-echo images. *Radiology*. 2018;286(3):948–59.
- Naraghi A, White LM. Three-dimensional MRI of the musculoskeletal system. *Am J Roentgenol*. 2012;199:283–93.
- Ma J. A single-point Dixon technique for fat-suppressed fast 3D gradient-echo imaging with a flexible echo time. *J Magn Reson Imaging*. 2008;27(4):881–90.
- Guerini H, Omoumi P, Guichoux F, Vuillemin V, Morvan G, Zins M, et al. Fat suppression with Dixon techniques in musculoskeletal magnetic resonance imaging: a pictorial review. *Semin Musculoskelet Radiol*. 2015;335–47.
- Del Grande F, Santini F, Herzka DA, Aro MR, Dean CW, Gold GE, et al. Fat-suppression techniques for 3-T MR imaging of the musculoskeletal system. *Radiographics*. 2014;34(1):217–33.
- Maas M, Dijkstra PF, Akkerman EM. Uniform fat suppression in hands and feet through the use of two-point Dixon chemical shift MR imaging. *Radiology*. 1999;210(1):189–93.
- Park HJ, Lee SY, Choi SH, Hong HP, Choi YJ, Kim MS. Reduced metallic artefacts in 3T knee MRI using fast spin-echo multi-point Dixon compared to fast spin-echo T2-weighted sequences. *Clin Radiol*. 2017;72(11):996.e1–6.
- Lee S, Choi D, Shin H, Baek H, Choi H, Park S. FSE T2-weighted two-point Dixon technique for fat suppression in the lumbar spine: comparison with SPAIR technique. *Diagnostic Interv Radiol*. 2018;24:175–80.
- Brandão S, Seixas D, Ayres-Basto M, Castro S, Neto J, Martin C, et al. Comparing T1-weighted and T2-weighted three-point Dixon technique with conventional T1-weighted fat-saturation and short-tau inversion recovery (STIR) techniques for the study of the lumbar spine in a short-bore MRI machine. *Clin Radiol*. 2013;68(11):e617–23.
- Reeder SB, Yu H, Johnson JW, Shimakawa A, Brittain JH, Pelc NJ, et al. T1- and T2-weighted fast spin-echo imaging of the brachial plexus and cervical spine with IDEAL water–fat separation. *J Magn Reson Imaging*. 2006;24(4):825–32.
- Rybicki FJ, Chung T, Reid J, Jaramillo D, Mulkern RV, Ma J. Fast three-point Dixon MR imaging using low-resolution images for phase correction: a comparison with for pediatric musculoskeletal imaging. *Am J Roentgenol*. 2001;177:1019–23.
- Kirchgesner T, Perlepe V, Michoux N, Larbi A, Vande BB. Fat suppression at three-dimensional T1-weighted MR imaging of the hands: Dixon method versus CHESSE technique. *Diagn Interv Imaging*. 2018;99:23–8.
- Wehrli F, Perkins T, Shimakawa A, Roberts F. Chemical shift-induced amplitude modulations in images obtained with gradient refocusing. *Magn Reson Imaging*. 1987;5(2):157–8.
- Bley TA, Wieben O, François CJ, Brittain JH, Reeder SB. Fat and water magnetic resonance imaging. *J Magn Reson Imaging*. 2010;31(1):4–18.
- Eggers H, Börnert P. Chemical shift encoding-based water-fat separation methods. *J Magn Reson Imaging*. 2014;40(2):251–68.
- Prince C, Oesingmann N, McGorty K, Lee V. Optimization of in-phase and opposed phase imaging at 3T for abdominal MRI. *Proc Intl Soc Mag Reson Med*. 2007;184(6):3837.
- Grimm A, Meyer H, Nickel MD, Nittka M, Raithel E, Chaudry O, et al. Evaluation of 2-point, 3-point, and 6-point Dixon magnetic resonance imaging with flexible echo timing for muscle fat quantification. *Eur J Radiol*. 2018;103:57–64.
- Ma J, Son JB, Bankson JA, Stafford RJ, Choi H, Ragan D. A fast spin echo two-point Dixon technique and its combination with sensitivity encoding for efficient T2-weighted imaging. *Magn Reson Imaging*. 2005;23(10):977–82.
- Weishaupt D, Köchli VD, Marincek B. How does MRI work: an introduction to the physics and function of magnetic resonance imaging. 2nd edition. Berlin Heidelberg: Springer; 2008.
- Park H, Lee SY, Rho MH, Chung EC, Ahn JH, Park JH, et al. Usefulness of the fast spin-echo three-point Dixon (mDixon) image of the knee joint on 3.0T MRI: comparison with conventional fast spin-echo T2-weighted image. *Br J Radiol*. 2016;89(1062):20151074.
- Kohl CA, Chivers FS, Lorans R, Roberts CC, Kransdorf MJ. Accuracy of chemical shift MR imaging in diagnosing indeterminate bone marrow lesions in the pelvis: review of a single institution's experience. *Skeletal Radiol*. 2014;43(8):1079–84.
- Zajick DC, Morrison WB, Schweitzer ME, Parellada JA, Carrino JA. Benign and malignant processes: normal values and differentiation with chemical shift MR imaging in vertebral marrow. *Radiology*. 2007;237(2):590–6.
- Douis H, Davies AM, Jeys L, Sian P. Chemical shift MRI can aid in the diagnosis of indeterminate skeletal lesions of the spine. *Eur Radiol*. 2016;26(4):932–40.
- Geith T, Schmidt G, Biffar A, Dietrich O, Dürr H, Reiser M, et al. Comparison of qualitative and quantitative evaluation of diffusion-weighted MRI and chemical-shift imaging in the differentiation of benign and malignant vertebral body fractures. *Am J Roentgenol*. 2012;199(5):1083–92.
- Zampa V, Cosottini M, Michelassi MC, Ortori S, Bruschini L, Bartolozzi C. Value of opposed-phase gradient-echo technique in distinguishing between benign and malignant vertebral lesions. *Eur Radiol*. 2002;12(7):1811–8.
- Costa F, Canella C, Viera F, Vianna E, Meohas W, Marchiori E. The usefulness of chemical-shift magnetic resonance imaging for the evaluation of osteoid osteoma. *Radiol Bras*. 2018;51(3):156–61.
- Schmeel FC, Luetkens JA, Wagenhäuser PJ, Meier-Schroers M, Kuetting DL, Feißt A, et al. Proton density fat fraction (PDFF) MRI for differentiation of benign and malignant vertebral lesions. *Eur Radiol*. 2018;28(6):2397–405.
- Schmeel FC, Luetkens JA, Enkirch SJ, Feißt A, Endler CH, Schmeel LC, et al. Proton density fat fraction (PDFF) MR imaging for differentiation of acute benign and neoplastic compression fractures of the spine. *Eur Radiol*. 2018;28(12):5001–9.
- Schmeel FC, Luetkens JA, Feißt A, Enkirch SJ, Endler CH, Wagenhäuser PJ, et al. Quantitative evaluation of T2* relaxation times for the differentiation of acute benign and malignant vertebral body fractures. *Eur J Radiol*. 2018;108:59–65.

34. Pezeshk P, Alian A, Chhabra A. Role of chemical shift and Dixon based techniques in musculoskeletal MR imaging. *Eur J Radiol.* 2017;94:93–100.
35. Suh CH, Yun SJ, Jin W, Park SY, Ryu C-W, Lee SH. Diagnostic performance of in-phase and opposed-phase chemical-shift imaging for differentiating benign and malignant vertebral marrow lesions: a meta-analysis. *Am J Roentgenol.* 2018;211(4):188–97.
36. Carroll KW, Feller JF, Tirman PFJ. Useful internal standards for distinguishing infiltrative marrow pathology from hematopoietic marrow at MRI. *J Magn Reson Imaging.* 1997;7(2):394–8.
37. El-Samie HAEKA, El-Ghany HSA. The value of added opposed/in phase MRI sequences in characterization of the focal vertebral bone marrow lesions in oncology patients. *Egypt J Radiol Nucl Med.* 2015;46(3):727–32.
38. Hwang S, Panicek DM. Magnetic resonance imaging of bone marrow in oncology. *J. Skeletal Radiol.* 2007;36(10):913–20.
39. Malkiewicz A, Dziedzic M. Bone marrow reconversion—imaging of physiological changes in bone marrow. *Polish J Radiol.* 2012;77(4):45–50.
40. Shiga NT, Del Grande F, Lardo O, Fayad LM. Imaging of primary bone tumors: determination of tumor extent by non-contrast sequences. *Pediatr Radiol.* 2013;43(8):1017–23.
41. Kenneally BE, Gutowski CJ, Reynolds AW, Morrison WB, Abraham JA. Utility of opposed-phase magnetic resonance imaging in differentiating sarcoma from benign bone lesions. *J Bone Oncol.* 2015;4(4):110–4.
42. Del Grande F, Farahani SJ, Carrino JA, Chhabra A. Bone marrow lesions: a systematic diagnostic approach. *Indian J Radiol Imaging.* 2014;24(3):279–88.
43. Kim YP, Kannengiesser S, Paek MY, Kim S, Chung TS, Yoo YH, et al. Differentiation between focal malignant marrow-replacing lesions and benign red marrow deposition of the spine with T2*-corrected fat-signal fraction map using a three-echo volume interpolated breath-hold gradient echo Dixon sequence. *Korean J Radiol.* 2014;15(6):781–91.
44. Disler D, Mccauley TR, Ratner LM, Kesack C, Cooper JA. In-phase and out-of-phase MR imaging of bone marrow: prediction of neoplasia based on the detection of coexistent fat and water. *Am J Roentgenol.* 1997;169:1439–47.
45. Kumar NM, Ahlawat S, Fayad LM. Chemical shift imaging with in-phase and opposed-phase sequences at 3T: what is the optimal threshold, measurement method, and diagnostic accuracy for characterizing marrow signal abnormalities? *Skeletal Radiol.* 2018;47(12):1661–71.
46. Shah L, Hanrahan C. MRI of spinal bone marrow. I Techniques and normal age-related appearances. *Am J Roentgenol.* 2011;197:1298–308.
47. Fayad L, Jacobs M, Wang X, Carrino J, Bluemke D. Musculoskeletal tumors: how to use anatomic, functional, and metabolic MR techniques. *Radiology.* 2012;265(2):340–56.
48. Shigematsu Y, Hirai T, Kawanaka K, Shiraishi S, Yoshida M, Kitajima M, et al. Distinguishing imaging features between spinal hyperplastic hematopoietic bone marrow and bone metastasis. *Am J Neuroradiol.* 2014;35(10):2013–20.
49. Chow LTC, Ng AWH, Wong SKC. Focal nodular and diffuse haematopoietic marrow hyperplasia in patients with underlying malignancies: a radiological mimic of malignancy in need of recognition. *Clin Radiol.* 2017;72(3):265.e7–265.e23.
50. Yoo HJ, Hong SH, Kim DH, Choi JY, Chae HD, Jeong BM, et al. Measurement of fat content in vertebral marrow using a modified Dixon sequence to differentiate benign from malignant processes. *J Magn Reson Imaging.* 2017;45(5):1534–44.
51. Gaudino S, Martucci M, Colantonio R, Lozupone E, Visconti E, Leone A, et al. A systematic approach to vertebral hemangioma. *Skeletal Radiol.* 2015;44(1):25–36.
52. Usmani S, Marafi F, Rasheed R, Al Kandari F, Ahmed N. Atypical hemangioma mimicking metastasis on 18F-sodium fluoride positron emission tomography-computed tomography and magnetic resonance imaging: gallium-68-prostate-specific membrane antigen positron emission tomography improves the specificity of bone lesions. *Indian J Nucl Med.* 2018;33(2):171–3.
53. Morales K, Arevalo-Perez J, Peck K, Holodny A, Lis E, Karimi S. Differentiating atypical hemangiomas and metastatic vertebral lesions: the role of T1-weighted dynamic contrast-enhanced MRI. *Am J Neuroradiol.* 2018;39(5):968–73.
54. Shi Y, Li X, Zhang X, Liu Y, Tang L, Sun Y-S. Differential diagnosis of hemangiomas from spinal osteolytic metastases using 3.0 T MRI: comparison of T1-weighted imaging, chemical-shift imaging, diffusion-weighted and contrast-enhanced imaging. *Oncotarget.* 2017;8(41):71095–104.
55. Kim DH, Yoo HJ, Hong SH, Choi JY, Chae HD, Chung BM. Differentiation of acute osteoporotic and malignant vertebral fractures by quantification of fat fraction with a Dixon MRI sequence. *Am J Roentgenol.* 2017;209(6):1331–9.
56. Cicala D, Briganti F, Casale L, Rossi C, Cagini L, Cesarano E, et al. Atraumatic vertebral compression fractures: differential diagnosis between benign osteoporotic and malignant fractures by MRI. *Musculoskelet Surg.* 2013;97(2):S169–79.
57. Mauch J, Carr C, Cloft H, Diehn F. Review of the imaging features of benign osteoporotic and malignant vertebral compression fractures. *Am J Neuroradiol.* 2018;39(9):1584–92.
58. Eito K, Waka S, Naoko N, Makoto A, Atsuko H. Vertebral neoplastic compression fractures: assessment by dual-phase chemical shift imaging. *J Magn Reson Imaging.* 2004;20(6):1020–4.
59. Erly WK, Oh ES, Outwater EK. The utility of in-phase/opposed-phase imaging in differentiating malignancy from acute benign compression fractures of the spine. *Am J Neuroradiol.* 2006;27(6):1183–8.
60. Ragab Y, Emad Y, Gheita T, Mansour M, Abou-Zeid A, Ferrari S, et al. Differentiation of osteoporotic and neoplastic vertebral fractures by chemical shift {in-phase and out-of phase} MR imaging. *Eur J Radiol.* 2009;72(1):125–33.
61. Del Grande F, Tatizawa-Shiga N, Farahani SJ, Chalian M, Fayad LM. Chemical shift imaging: preliminary experience as an alternative sequence for defining the extent of a bone tumor. *Quant Imaging Med Surg.* 2014;4(3):173–80.
62. Saifuddin A, Sharif B, Gerrand C, Whelan J. The current status of MRI in the pre-operative assessment of intramedullary conventional appendicular osteosarcoma. *Skeletal Radiol.* 2018;48(4):503–16.
63. Bray TJP, Singh S, Latifoltojar A, Rajesparan K, Rahman F, Narayanan P, et al. Diagnostic utility of whole body Dixon MRI in multiple myeloma: a multi-reader study. *PLoS One.* 2017;12(7):e0180562.
64. Dutoit JC, Verstraete KL. MRI in multiple myeloma: a pictorial review of diagnostic and post-treatment findings. *Insights Imaging.* 2016;7:553–69.
65. Vanel D, Casadei R, Alberghini M, Razgallah M, Busacca M, Albisinni U. MR imaging of bone metastases and choice of sequence: spin echo, in-phase gradient echo, diffusion, and contrast medium. *Semin Musculoskelet Radiol.* 2009;1(212):97–103.
66. O’Sullivan GJ, Carty FL, Cronin CG. Imaging of bone metastasis: an update. *World J Radiol.* 2015;7(8):202–12.
67. Hahn S, Lee Y, Suh J. Detection of vertebral metastases: a comparison between the modified Dixon turbo spin echo T2 weighted MRI and conventional T1 weighted MRI: a preliminary study in a tertiary centre. *Br J Radiol.* 2018;91(1085):20170782.
68. Ohno S, Togami I, Sei T, Ida K, Tsunoda M, Yamaoka K, et al. MR imaging of vertebral metastases at 0.2 Tesla: clinical evaluation of T1-weighted opposed-phase gradient-echo imaging. *Physiol Chem Phys Med NMR.* 2003;35(2):145–56.

69. Woolf DK, Padhani AR, Makris A. Assessing response to treatment of bone metastases from breast cancer: what should be the standard of care? *Ann Oncol*. 2015;26(6):1048–57.
70. Wu Q, Yang R, Zhou F, Hu Y. Comparison of whole-body MRI and skeletal scintigraphy for detection of bone metastatic tumors: a meta-analysis. *Surg Oncol*. 2013;22(4):261–6.
71. Morone M, Bali MA, Tunariu N, Messiou C, Blackledge M, Grazioli L, et al. Whole-body MRI: current applications in oncology. *Am J Roentgenol*. 2017;209:336–49.
72. Petralia G, Padhani AR. Whole-body magnetic resonance imaging in oncology: uses and indications. *Magn Reson Imaging Clin N Am*. 2018;26(4):495–507.
73. Stecco A, Trisoglio A, Soligo E, Berardo S, Sukhovei L, Carriero A. Whole-body MRI with diffusion-weighted imaging in bone metastases: a narrative review. *Diagnostics (Basel)*. 2018. <https://doi.org/10.3390/diagnostics8030045>.
74. Guimarães MD, Noschang J, Teixeira SR, Santos MK, Lederman HM, Tostes V, et al. Whole-body MRI in pediatric patients with cancer. *Cancer Imaging*. 2017;17(6):1–12.
75. Ma J, Costelloe CM, Madewell JE, Hortobagyi GN, Green MC, Cao G, et al. Fast Dixon-based multisequence and multiplanar MRI for whole-body detection of cancer metastases. *J Magn Reson Imaging*. 2009;29(5):1154–62.
76. Costelloe CM, Kundra V, Ma J, Chasen BA, Rohren EM, Bassett RL, et al. Fast Dixon whole-body MRI for detecting distant cancer metastasis: a preliminary clinical study. *J Magn Reson Imaging*. 2012;35(2):399–408.
77. Costelloe CM, Madewell JE, Kundra V, Harrell RK, Bassett RL, Ma J. Conspicuity of bone metastases on fast Dixon-based multisequence whole-body MRI: clinical utility per sequence. *Magn Reson Imaging*. 2013;31(5):669–75.
78. Nichols RE, Dixon LB. Radiographic analysis of solitary bone lesions. *Radiol Clin NA*. 2011;49(6):1095–114.
79. Costelloe CM, Madewell J. Radiography in the initial diagnosis of primary bone tumors. *Am J Neuroradiol*. 2013;200:3–7.
80. Stacy GS, Mahal RS, Peabody TD. Staging of bone tumors: a review with illustrative examples. *Am J Roentgenol*. 2006;186(4):967–76.
81. Nascimento D, Suchard G, Hatem M, de Abreu A. The role of magnetic resonance imaging in the evaluation of bone tumours and tumour-like lesions. *Insights Imaging*. 2014;5(4):419–40.
82. Alyas F, James S, Davies A, Saifuddin A. The role of MR imaging in the diagnostic characterisation of appendicular bone tumours and tumour-like conditions. *Eur Radiol*. 2007;17(10):2675–86.
83. Khoo MMY, Saifuddin A. The role of MRI in image-guided needle biopsy of focal bone and soft tissue neoplasms. *Skeletal Radiol*. 2013;42(7):905–15.
84. Oei L, Koromani F, Rivadeneira F, Zillikens MC, Oei EHG. Quantitative imaging methods in osteoporosis. *Quant Imaging Med Surg*. 2016;6(6):680–98.
85. He J, Fang H, Li X. Vertebral bone marrow fat content in normal adults with varying bone densities at 3T magnetic resonance imaging. *Acta Radiol*. 2019;60(4):509–15.
86. Zhao Y, Huang M, Ding J, Zhang X, Spuhler K, Hu S, et al. Prediction of abnormal bone density and osteoporosis from lumbar spine MR using modified Dixon quant in 257 subjects with quantitative computed tomography as reference. *J Magn Reson Imaging*. 2019;49(2):390–9.
87. Glover GH, Schneider E. Three-point Dixon technique for true water/fat decomposition with B0 inhomogeneity correction. *Magn Reson Med*. 1991;18(2):371–83.
88. Yoo YH, Kim H, Lee YH, Yoon C, Paek MY, Yoo H, et al. Comparison of multi-echo Dixon methods with volume interpolated breath-hold gradient echo magnetic resonance imaging in fat-signal fraction quantification of paravertebral muscle. *Korean J Radiol*. 2015;16(5):1086–95.
89. Swartz PG, Roberts CC. Radiological reasoning: bone marrow changes on MRI. *Am J Roentgenol*. 2009;193:1–4.

Publisher's note Springer Nature remains neutral with regard to jurisdictional claims in published maps and institutional affiliations.